

# Design and Analysis of a Compact Wideband Monopole Patch Antenna for Future Handheld Gadgets

Abhishek K. Chaudhary\* and Murli Manohar

**Abstract**—In this article, a compact super wideband (SWB) monopole antenna with a wide-frequency is designed and analyzed for future handheld gadgets. The designed antenna is made by etching four slots on a round cornered rectangular patch which are connected through a 50- $\Omega$  triangular tapered microstrip transmission feedline (TTMTF) for broadband impedance matching. A triangular slot is etched on the semicircular partial ground plane, which helps to shift the lower frequency edge of 1.07 GHz to 1 GHz. The experimental results show that the proposed antenna operates over a wide frequency range of 1–30 GHz with a reflection coefficient of less than  $-10$  dB. The antenna acquires a compact dimension of  $25 \times 16 \times 0.787$  mm<sup>3</sup>. Further, an equivalent circuit method is used to analyze the proposed structure, and its outcome is compared with the simulated and experimental results. The peak gain of the designed antenna is about 5.5 dBi. The proposed antenna has low cross-polarization even at higher frequencies. Finally, the time domain analysis is also carried out to see the distortion between transmitting and receiving modes. The designed antenna can be used for various wireless applications such as NB-IoT, GPS, Wi-BRO, ISM band, IRNSS, WiMAX, X-band, Ku-band, and K-band.

## 1. INTRODUCTION

In the recent epoch of wireless technology, printed monopole antennas are in high demand due to their numerous desirable features such as wideband characteristics, compact in size, high speed data communication, and omnidirectional radiation characteristics [1, 2]. Owing to all these attributes, printed monopole antennas are presently under consideration for SWB applications. The ratio bandwidth of more than 10 : 1 impedance bandwidth is usually named as super wideband [3]. SWB antenna provides an enormously huge bandwidth as compared to an ultra-wideband (UWB) (3.1 to 10.6 GHz with a bandwidth ratio of 3.4 : 1 [4]) antenna, motivating the authors to investigate SWB antenna (can cater multiservices). Subsequently, the design of SWB miniaturized antennas while upholding wideband features is a challenging task in the area of modern wireless system, especially for radar surveillance, electronics hand-held gadgets, mobile and Internet of military things (IOMT) applications [5]. Therefore, currently several researchers are concentrating on obtaining a tradeoff between bandwidth enhancement and antenna size miniaturization.

Over the past few years, many researchers have given their valuable contribution to the design of various SWB antennas [6–16]. In [6], Dong et al. reported a printed tapered microstrip line fed monopole SWB antenna having a dimension of  $150 \times 156$  mm<sup>2</sup>. The antenna was implemented by merging a one half-disc and one half-ellipse to cover 0.4–16 GHz. In [7], a tree-shaped third iterative elliptical monopole antenna with a semi-elliptical ground is investigated which has a fractional bandwidth of 54.78 : 1 (0.65–35.61 GHz) with a physical configuration of  $170 \times 150$  mm<sup>2</sup>. An asymmetric co-planar fed hexagonal loop strip antenna with a boomerang-shaped ground plane was studied in [8]. This antenna exhibited a frequency spectrum of 1.18–49.22 GHz with a total foot print of  $103.05 \times 72.5$  mm<sup>2</sup>. An M-shaped Vivaldi array antenna with a physical dimension of  $160 \times 100$  mm<sup>2</sup> is studied in [9]. The designed antenna

---

Received 24 December 2020, Accepted 2 February 2021, Scheduled 13 February 2021

\* Corresponding author: Abhishek Kumar Chaudhary (achaudhary@iiitmanipur.ac.in).

The authors are with the Indian Institute of Information Technology Senapati, Manipur, India.

supports the frequency range from 3.25 to 8.75 GHz with a bandwidth and peak gain of 5.6 GHz and 16.4 dBi, respectively. In [10], a maple leaf-shaped radiating element with a truncated ground plane was designed to attain UWB characteristics. The overall configuration of the antenna was  $33 \times 34 \text{ mm}^2$  with a frequency band of 1.7 to 11.1 GHz. The design and analysis of a triple-notched band maple leaf-shaped UWB antenna with a partial ground plane were studied in [11] to cover an impedance bandwidth of 1.4–11.3 GHz. In [12], the designed monopole antenna was made by merging four elliptical patches having a frequency band of 1.9 to 30 GHz and covering multiple wireless applications such as wireless local area network, C-band, K-band, Ku-band, and wireless USB applications with a physical dimension of  $50 \times 40 \text{ mm}^2$ . A monopole antenna fed by a triangular tapered feedline with a defected ground plane was reported in [13] for wideband applications (3–50 GHz). This antenna is suitable for the C-band and X-band applications. An octagonal-ring shaped monopole antenna was designed in [14] to cover an operating bandwidth of 2.59–31.14 GHz, and its impedance bandwidth was enhanced by adding a stub at the top right corner with the main patch. In [15], a two iterations based Sierpinski square slotted hexagonal fractal antenna fed by coplanar waveguide was presented to achieve an impedance bandwidth of 3.4–37.4 GHz. A semicircular radiator with trapezoidal ground plane was presented in [16] with bandwidth dimension ratio (BDR) of 4261 for 15.38 : 1 of ratio bandwidth.

However, the above mentioned antennas are either large or do not cover important low frequency wireless communication services such as 600 MHz 5G, GPS, GSM 1800, WiMAX, WLAN, and 4G. Recently, many compact SWB antennas have been published in the literature [17–20]. In [17], a miniaturized antenna with a size of  $40 \times 25 \text{ mm}^2$  was investigated whose realized peak gain was 4.25 dBi for resonating frequency 0.9–22.35 GHz. Miniaturization was obtained by truncating corners and modifying edges of the patch. An elliptical guitar-shaped monopole radiator with triple band-notched characteristics mentioned in [18] had an operational gain of 2.2–6.88 dBi ranging from 2.76 to 39.53 GHz. The antenna compactness (overall dimensions of  $32 \times 27 \text{ mm}^2$ ) was achieved by combining four ellipses having an eccentricity ratio of 0.5. In [19], a crescent-shaped compact radiator ( $32 \times 22 \text{ mm}^2$ ) with a partially slotted ground plane was designed to operate from 2.5 to 29 GHz, which attained a peak gain of 6.1 dBi. A compact SWB patch antenna based on diversities of reactive loaded technique was reported in [20] where by employing U-shaped slot and complement U-slot on the radiating patch, an SWB characteristic was enabled from 2.43 to 32.93 GHz with a gain variation of 2.73 to 7.35 dBi. The antenna occupied a total foot print of  $26 \times 25 \text{ mm}^2$ . Although the antennas reported in [17–20] are relatively small in size, most of the antennas have reasonably low gain. Typically, the antenna with high gain is useful for increasing the range of a line-of-sight path.

It is well known that the integral relation between lower frequency and antenna dimension compels antenna researchers to conciliate with antenna gain and bandwidth. Therefore, in this communication a novel broadband printed monopole antenna with high gain, compact size, and large BDR has been investigated. A radiating patch is realized by etching four slots on a round cornered rectangular patch. To improve the impedance matching between source and load (radiating patch), a TTMTF is employed. Further, the lower edge of the main radiator (beside RF front end) is modified from sharp corner to curvature to prevent an evolutionary change in impedance at the conjunction of patch and feed line. The proposed antenna covers a wide spectrum band of 1 to 30 GHz with small space and can be integrated with numerous devices such as smart phones, laptops, personal computers, satellite communication, Internet of things (IOTs), and wireless modems. The simulation results of the designed antenna are accomplished by Ansoft high-frequency structure simulator (HFSS) software and compared with the measured and analytical results. The proposed structure is small in size and has low cross-polarization not only at lower frequencies but also at higher frequencies than other SWB antennas [19, 21]. The measured gain of the proposed antenna varies from 0.1 to 5.6 dBi.

## 2. STRUCTURAL ANALYSIS OF PROPOSED ANTENNA

### 2.1. Antenna Layout

The layout of the proposed antenna fed by a  $50\text{-}\Omega$  TTMTF is presented in Fig. 1. The designed antenna is implemented on a 0.787-mm-thick Roger RT/duroid 5870 substrate which makes the exemplary antenna applicable up to millimeter frequency range with low loss. The overall volume of the proposed antenna is about  $25 \times 16 \times 0.787 \text{ mm}^3$  and is easily mounted on the restricted space provided by the modern tiny

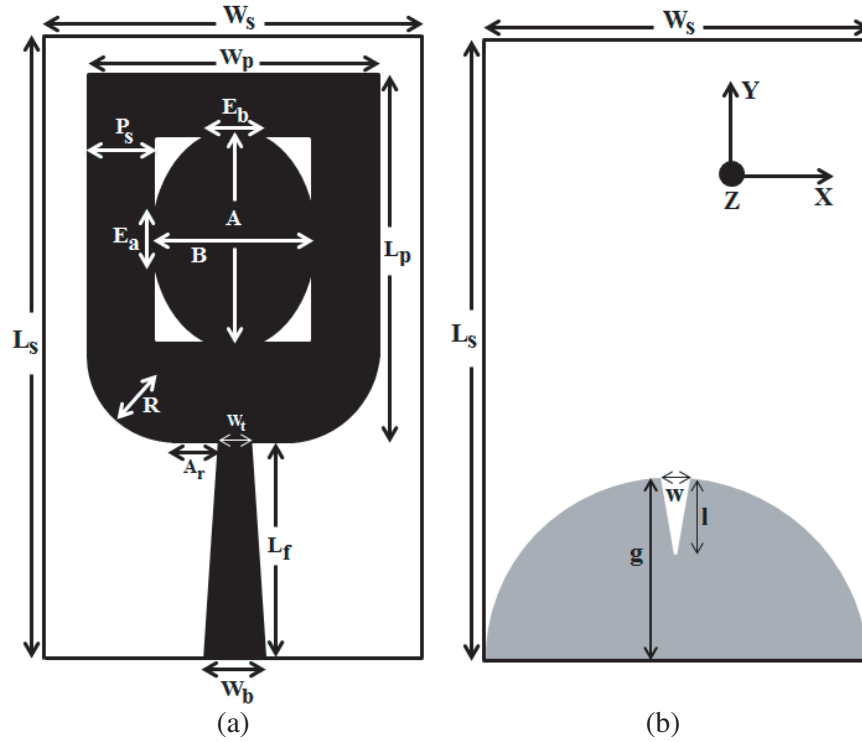


**Figure 1.** Layout of proposed antenna. (a) Top view. (b) Bottom view.

mobile phones. As can be seen in Fig. 1, the designed antenna is made by inserting four slots in the rectangular patch. Additionally, the lower edge of the slot loaded rectangular patch is modified from sharp corner to curvature for smooth current's path. A 50-Ω TTMTF is utilized to feed the antenna for broadband impedance matching, because triangular tapered precludes the formation of fictitious reflections as well as evanescent modes which enable us to have smooth impedance transition from one line to another line. A triangular slot with a dimension of  $3.2 \times 0.5 \text{ mm}^2$  is etched on the semi-circular ground plane which results in further shifting the lower-frequency edge towards the lower frequency. Hence, an enormously wideband radiation characteristic can be achieved throughout the operational band. The optimized dimensions of the proposed antenna are given as  $L_s = 25 \text{ mm}$ ,  $W_s = 16 \text{ mm}$ ,  $L_p = 15 \text{ mm}$ ,  $W_p = 12 \text{ mm}$ ,  $A = 8 \text{ mm}$ ,  $B = 6 \text{ mm}$ ,  $E_a = 2 \text{ mm}$ ,  $E_b = 2.56 \text{ mm}$ ,  $P_s = 3 \text{ mm}$ ,  $A_r = 1.5 \text{ mm}$ ,  $W_t = 1 \text{ mm}$ ,  $R = 2.85 \text{ mm}$ ,  $L_f = 8 \text{ mm}$ ,  $W_b = 2 \text{ mm}$ ,  $g = 7.7 \text{ mm}$ ,  $w = 0.46 \text{ mm}$ , and  $l = 3.2 \text{ mm}$ . The length of the TTMTF is optimized by Riccati equation which describes the voltage reflection coefficient equation given in [21].

$$\Gamma = \frac{1}{2} e^{-j\beta L} \ln \left( \frac{Z_L}{Z_0} \right) \left[ \frac{\sin(\beta L/2)}{\beta L/2} \right]^2 \quad (1)$$

where  $\Gamma$  represents the reflection coefficient;  $L$  is the length of the feed line;  $Z_L$  and  $Z_0$  represent the load and characteristic impedance, respectively; and  $\beta$  represents the phase constant.

For the rectangular patch, the estimation of lower frequency can be finalized using the mathematical expression (2) [21]

$$f_L = \frac{7.2}{L_p + K/2\pi L_p + p} \text{ GHz} \quad (2)$$

where  $f_L$  shows the lower frequency of the antenna;  $L_p$  is the length of the patch;  $K$  represents the area of the rectangular radiating patch; and  $p$  denotes the gap between radiating patch and ground plane. The lower frequency of the proposed antenna is calculated by substituting the values of  $L_p$ ,  $K$ , and  $p$  in Eq. (2).

## 2.2. Antenna Optimization Process

The design modifications of the proposed antenna are shown in Fig. 2, which comprises five distinct antennas to acquire the optimized SWB antenna. Fig. 3 represents the simulated reflection coefficient against frequency characteristics for the five different antennas. The proposed antenna is investigated starting with a simple rectangular patch (Antenna 1) fed by a rectangular feedline structure and rectangular ground conductor, whereas its response is given in Fig. 3. It can be seen that the performance of Antenna 1 is not satisfactory in the frequency range of 4–24 GHz. Also, the bandwidth is quite small for the reflection coefficient of less than  $-10$  dB. In the second evolution, four identical arc-shaped triangular slots are etched on the rectangular monopole antenna, and at the same time, the rectangular feed line is replaced with a TTMTF. The combination of these provides a wide impedance bandwidth especially at frequencies beyond 18 GHz. Etching the slot on the conducting part results in increment of electrical length of the main radiator, but it does not cover UWB/SWB frequency band as shown in Fig. 3. The antenna with a round cornered rectangular patch (Antenna 3) creates an additional resonance especially at 2.5 GHz resulting in a broader bandwidth, but cannot cover the full X-band ( $S_{11}$  greater than  $-10$  dB from 7–10 GHz) communication services. In the next phase (Antenna 4), we modify the rectangular ground plane of Antenna 3 into a semicircular ground plane, i.e., Antenna 4. With this modification, slightly better matching can be accomplished at 8 GHz and hence maximizing the overall bandwidth (1.07 GHz–30 GHz) with a reasonably high gain. Finally, by injecting the triangular slot on the ground plane, an optimized SWB monopole antenna is designed, which further lowers the frequency from 1.07 to 1 GHz without enlarging optimized dimensions as shown in Fig. 3. This is owing to the electromagnetic coupling introduced between the slot loaded partial ground plane and TTMTF.

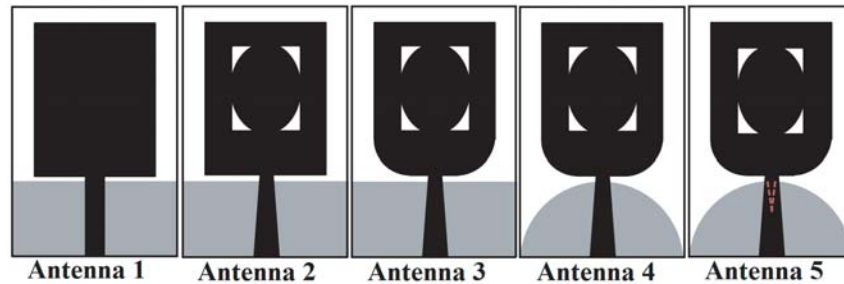


**Figure 2.** Design modifications of SWB antenna.

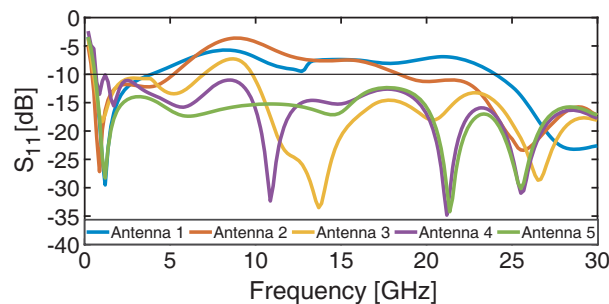


**Figure 3.** Simulated  $S_{11}$  vs frequency graph for different shaped antennas.

## 3. ANALYSIS OF PROPOSED ANTENNA USING EQUIVALENT CIRCUIT

To confirm the appropriateness of simulated reflection coefficient, the proposed structure is theoretically analyzed by using a lumped equivalent circuit consisting of elements like resistor, inductor, and capacitor. Electrical circuit including resonators have been proposed to understand the multiband/broadband behavior of handset antennas [22]. Foster canonical [23] technique can be used

to model the equivalent circuit diagram for both dipole and monopole antennas. In this model, the wide impedance bandwidth can be obtained owing to multiple resonances generated by the SWB patch antenna, and each resonance represents the parallel RLC resonating circuit. A Foster Canonical network based equivalent circuit for the proposed SWB monopole antenna for 12-resonating modes is shown in Fig. 4. The input impedance [23] of an equivalent circuit model can be written mathematically as

$$Z_{in}(\omega) \cong \sum_{Q=1}^n \frac{j\omega \cdot R_Q \cdot L_Q}{R_Q \cdot (1 - \omega^2 \cdot L_Q \cdot C_Q) + j\omega \cdot L_Q} \tag{3}$$

where  $R_Q$ ,  $C_Q$ , and  $L_Q$  ( $Q = 1$  to 12) are the values of resistance, capacitance, and inductance of each parallel R-L-C resonating circuit. The numerical quantity ‘ $n$ ’ shows the total number of resonating modes of the proposed antenna. To reduce the complexity, only the real part is contemplated to obtain the values of  $R_Q$ ,  $C_Q$ , and  $L_Q$  with the following formula [23]

$$R_{re} = \sum_{Q=1}^n \frac{R_Q}{1 + R_Q \cdot \left( \frac{1}{L_Q \cdot 2\pi f} - C_Q \cdot 2\pi f \right)^2} \tag{4}$$

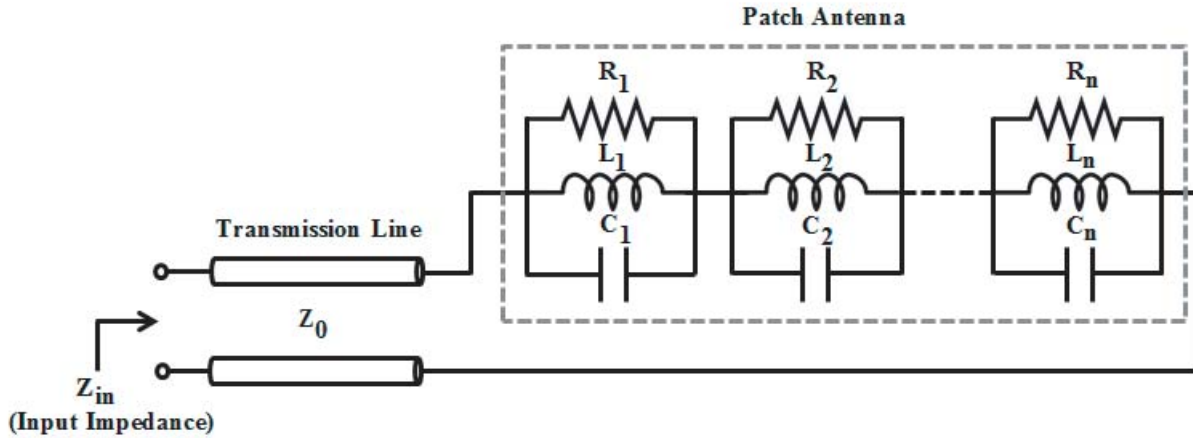


Figure 4. Foster Canonical network based equivalent circuit topology of the proposed antenna.

By using the above methods, the parameters ( $R_Q$ ,  $C_Q$ , and  $L_Q$ ) of the equivalent circuit can be obtained. Initially the values of  $R_1$ ,  $L_1$ , and  $C_1$  are calculated by using Eq. (4). In the next step, the equivalent circuit is constructed (12 resonators), altered, and optimized in advanced design system (ADS) software. The computed all the different parameters  $R_Q$ ,  $C_Q$ , and  $L_Q$  are tabulated in Table 1, and after that the input impedance is calculated using Equation (3). Finally, the return loss ( $S_{11}$ ) of the proposed antenna can be explored by

$$RL = -20 \log |\Gamma| \text{ dB} \tag{5}$$

where  $\Gamma$  (reflection coefficient) =  $(Z_{in} - Z_0)/(Z_{in} + Z_0)$  and  $Z_0$  (characteristics impedance of feedline) =  $50\Omega$ .

The theoretical and simulated return losses of the SWB antenna are presented in Fig. 5, which show a satisfactory agreement.

#### 4. PARAMETRIC ANALYSIS OF THE PROPOSED ANTENNA

##### 4.1. Optimization of Ground Plane with Different Value of $g$

An arch-shaped ground plane located on the back side of the radiating element is also responsible for matching the impedance over band of interest. Impedance matching variation with an alteration in  $g$

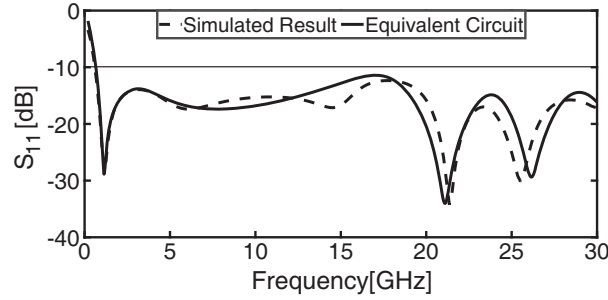


**Figure 5.** Simulated  $S_{11}$  vs frequency plot for analytical and simulated results.

**Table 1.** Parameter values of optimized Equivalent circuit diagram.

Number of resonating mode ( $Q = 1$ to 12)	Resistance ( $\Omega$ )	Inductance (pH)	Capacitance (pF)
$Q = 1$	$R_1 = 65.175$	$L_1 = 2.59$	$C_1 = 2.3$
$Q = 2$	$R_2 = 75.125$	$L_2 = 2.99$	$C_2 = 2.4$
$Q = 3$	$R_3 = 63.185$	$L_3 = 3.11$	$C_3 = 3$
$Q = 4$	$R_4 = 29.325$	$L_4 = 20.415$	$C_4 = 2.15$
$Q = 5$	$R_5 = 40.91$	$L_5 = 1294.07$	$C_5 = 1.7$
$Q = 6$	$R_6 = 33.715$	$L_6 = 10000.68$	$C_6 = 0.001$
$Q = 7$	$R_7 = 31.42$	$L_7 = 18.767$	$C_7 = 1.6$
$Q = 8$	$R_8 = 46.455$	$L_8 = 24.21$	$C_8 = 0.835$
$Q = 9$	$R_9 = 33.045$	$L_9 = 1.18$	$C_9 = 8.07$
$Q = 10$	$R_{10} = 42.885$	$L_{10} = 69.704$	$C_{10} = 1.1$
$Q = 11$	$R_{11} = 40.729$	$L_{11} = 7002.228$	$C_{11} = 6.22$
$Q = 12$	$R_{12} = 41.45$	$L_{12} = 19.25$	$C_{12} = 0.61$

is demonstrated in Fig. 6. From Fig. 6, one can observe that the optimized value of an arched-shaped ground plane length ( $g$ ) is 7.7 mm. As the value of  $g$  rises or falls from its optimal value, more power will be reflected from the load side, and hence the impedance becomes mismatched for the complete operational band. This is perhaps owing to increase or decrease of the inductive effect, which results in shifting the resonance towards right side.

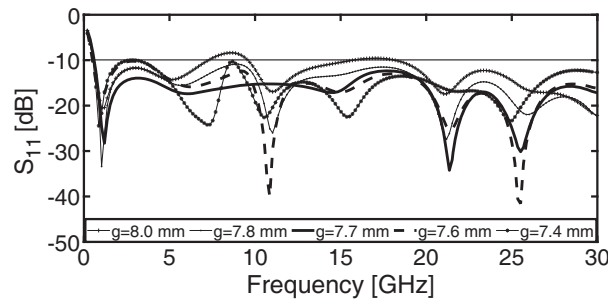


**Figure 6.** Simulated  $S_{11}$  vs frequency plot for different values of  $g$ .

#### 4.2. Effect of Etching Triangular Slot in the Conducting Ground Plane

In Fig. 7, we study the effect of the length ( $l$ ) and width ( $w$ ) of the triangular slot on  $S_{11}$ . It can be perceived from Fig. 7(a) that increasing or decreasing the triangular slot length  $l$  results in the reduction in reflection coefficient (around  $-10$  dB) at frequency 8 GHz, and hence the antenna fails to cover the SWB. However, the optimized value of  $l$  gives a reflection coefficient of much higher than  $-10$  dB at 8 GHz. Therefore, the value of  $l$  has been chosen as 3.2 mm for acquiring wideband impedance bandwidth. Fig. 7(b) displays the reflection coefficient against frequency graph for different values of  $w$ . As the width ( $w$ ) of the triangular slot decreases from 0.5 mm to 0.2 mm, the reflection coefficient becomes worse at 8 GHz. Moreover, the lower frequency edge of the antenna is shifted towards higher frequency end (i.e., from 1 to 1.8 GHz). Consequently, when the value of  $w$  decreases from 0.7 mm to 0.5 mm, the percentage bandwidth of the antenna increases from 186.4 to 187.1. This is because of the capacitive loading effect introduced by the slot loaded conducting ground plane, which nullifies the inductive loading effect of the main radiator to create approximately pure resistive antenna impedance and hence enhance the bandwidth. Therefore, optimal value of  $w$  is selected as 0.5 mm.

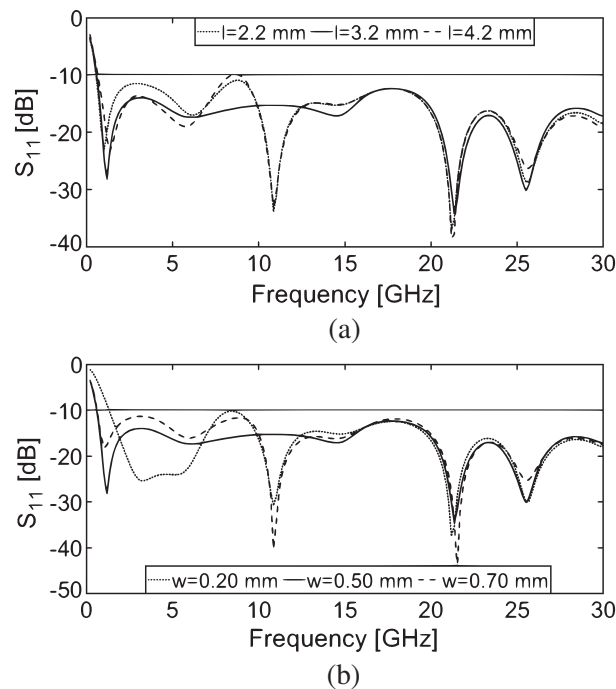


**Figure 7.** Simulated  $S_{11}$  vs frequency plot for various values of  $l$  and  $w$ .

#### 4.3. Effect of the Length of TTMTF on the Bandwidth

A TTMTF is used to match the impedance between the source and radiating patch and is optimized for maximizing the performance of impedance matching of the proposed antenna by means of varying  $L_f$  as shown in Fig. 8(a). As can be observed from Fig. 8(a), the length of the TTMTF makes a dramatic influence on the reflection coefficient graph especially at the lower frequency. When the value of  $L_f$  is increased or decreased, the impedance of lower frequencies becomes highly mismatched. Hence, in order to get the broadest  $-10$  dB impedance bandwidth through the desired band, a value of  $L_f$  is selected as 8 mm.

#### 4.4. Effect of the Round Cornered Rectangular Ring at Lower Frequency

In order to improve the matching performance at lower frequencies, the lower edge of the main radiator (beside RF front end) is modified from sharp corner to curvature. Therefore, in this section the radius

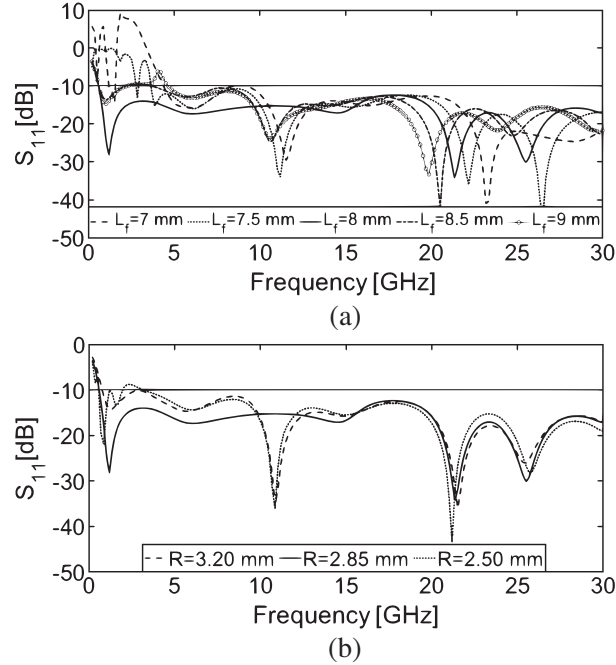


**Figure 8.** Simulated  $S_{11}$  vs frequency plot for various feedline length  $L_f$  and different values of  $R$ .

of the curvature for various values of  $R$  are considered as publicized in Fig. 8(b). From the figure one can be noticed that by increasing or decreasing the value of  $R$  from the optimized result ( $R = 2.85$  mm), there is an insignificant effect beyond 3.5 GHz. However, the performance of the antenna is deteriorated in the frequency band of 2–3.5 GHz, and it does not cover the important wireless communication services such as Wi-BRO and ISM band. At  $R = 2.85$  mm, the electrical current path length increases, and hence impedance matching tends to improve.

#### 4.5. Current Distribution Investigation

In order to examine the distributed current on the radiating patch, TTMTF, and ground plane, the simulated current distributions of frequencies 1.5, 12, 22, and 30 GHz are shown in Fig. 9. At frequency 1.5 GHz shown in Fig. 9(a), the concentrated surface current is high on the TTMTF as well as the lower edge of the main patch (near RF front end), which improves the antenna performance at low frequencies (1.5 GHz). At frequencies 12 and 22 GHz, the distributed current decreases on the TTMTF; however, the current density increases on the boundary of the main patch and the upper edge of the ground plane as shown in Fig. 9(b) and Fig. 9(c), respectively. As a consequence, several higher order generated modes overlap with the adjacent modes, and hence, enormously large bandwidth can be achieved. Fig. 9(d) shows the current distribution at 30 GHz. From the figure one can see that relatively large amount of current is clustered on the edge of the four arc-shaped slots and the main radiator; however, these currents are traveling almost horizontally, which results in the increase of the cross polarization at high frequencies. Moreover, at high frequencies the involvement of the ground plane in current distribution is more.

### 5. ANTENNA EXPERIMENTAL RESULTS

In the given section, we have measured the various parameters of the proposed SWB antenna for example reflection coefficient, peak gain, and radiation patterns. The front and back views of the fabricated antenna are presented in Fig. 10. Anritsu S820E Vector Network Analyser (VNA) is used to measure the fabricated antenna at microwave frequency. Fig. 11(a) represents the comparison of the simulated and measured reflection coefficients ( $S_{11} \leq -10$  dB) of the proposed printed monopole

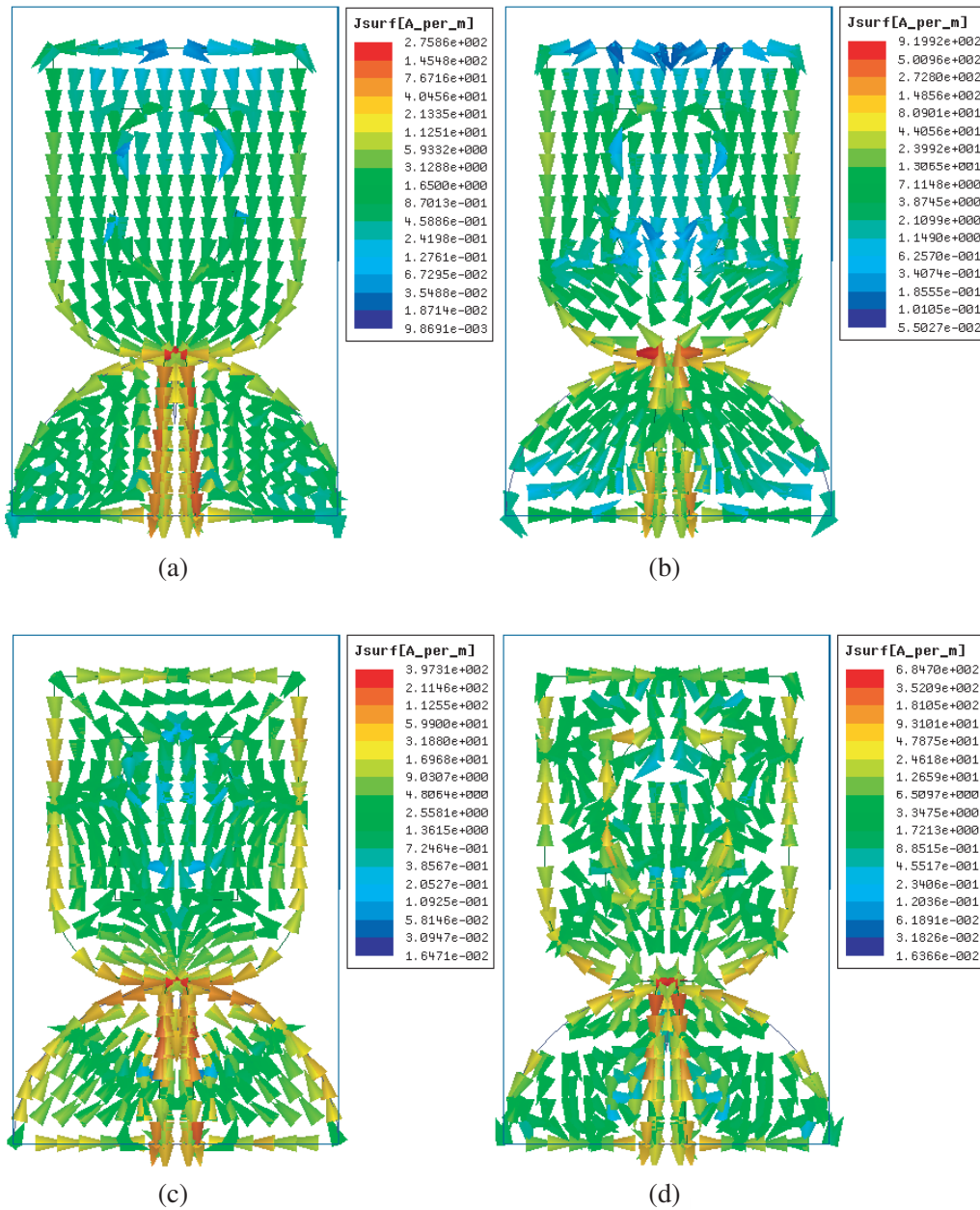


**Figure 9.** Simulated surface current distribution of the designed antenna at frequencies (a) 1.5 GHz, (b) 12 GHz, (c) 22 GHz, and (d) 30 GHz.

antenna. Measured reflection coefficient demonstrates that the presented antenna delivers  $-10$  dB bandwidth over the frequency band of 1–30 GHz which authenticates the usefulness of SWB applications. The measured and simulated peak gains of the proposed antenna are compared in Fig. 11(b). Gain of the proposed antenna is measured based on the Frii’s transmission formula given below

$$P_r = G_r G_t P_t \left( \frac{\lambda}{4\pi R} \right)^2 \tag{6}$$

where  $G_t$ ,  $G_r$ ,  $P_t$ ,  $P_r$ , and  $R$  are the transmitting antenna gain, receiving antenna gain, transmitted power, received power, and distance between two antennas, respectively. It can be observed from the figure that the measured gain variation in the frequency range of 1–30 GHz changes from 0.1 to 5 dBi

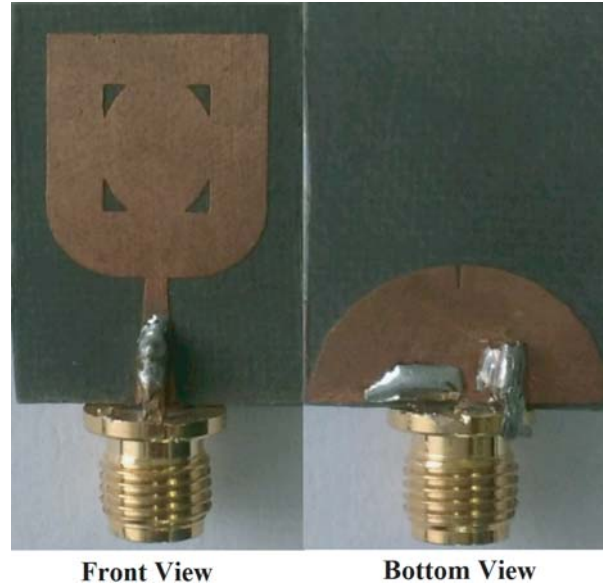


**Figure 10.** Fabricated portrait of the Proposed Antenna.

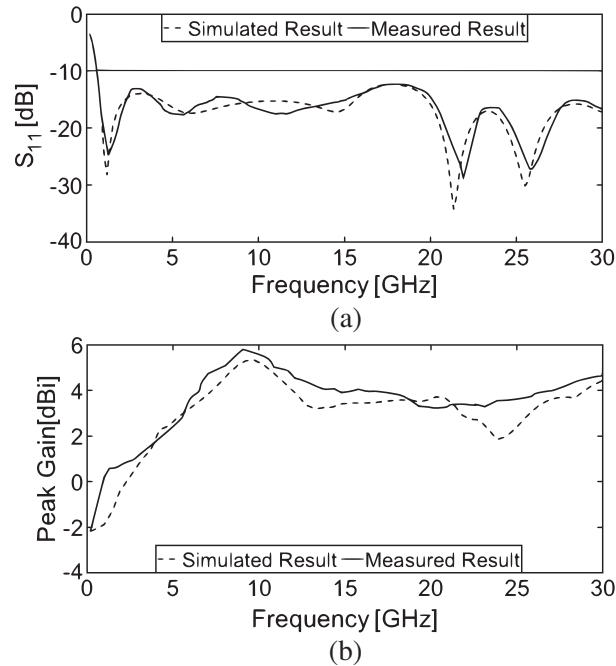


**Figure 11.** Simulated and Measured  $S_{11}$  characteristics and peak gain of the designed antenna.

with a peak gain of 5.5 dBi at 9 GHz, which shows that the presented antenna works well up to 30 GHz.

A key term bandwidth dimension ratio (BDR) is utilized to evaluate the compactness as well as the wideband characteristics of the antenna [24]. This index provides details of the size of the antenna concerning ratio of bandwidth (in percentage) to its electrical area unit, and it is represented by  $(\%/\lambda^2)$ .

$$BDR = \frac{\text{Bandwidth} (\%)}{(\lambda_{\text{length}} \times \lambda_{\text{width}})} \quad (7)$$

where  $\lambda$  represents the wavelength of the antenna at the lower-edge of the operating frequency that

meets the return loss of  $-10$  dB [24].  $\lambda_{length}$  and  $\lambda_{width}$  give the electrical length and width of the antenna with respect to lower-edge frequency. As the value of BDR increases, it is shown that the dimension of the antenna becomes compact, and the antenna has larger bandwidth. The performance comparisons between the proposed antenna and the existing antennas in terms of physical dimension, ratio BW, BDR, and gain are revealed in Table 2.

**Table 2.** Various parameters comparison of proposed antenna with recent published SWB antennas.

Ref.	Electrical Dimension	Ratio BW	$f_{low}$ [GHz]	BDR	Peak Gain [dBi]
[6]	$0.32\lambda \times 0.33\lambda$	25 : 1	0.64	1508.2	10
[7]	$0.32\lambda \times 0.37\lambda$	54.78 : 1	0.65	1628.6	6.51
[8]	$0.28\lambda \times 0.40\lambda$	41.7 : 1	1.18	1701.8	10.6
[9]	$1.08\lambda \times 1.73\lambda$	2.69 : 1	3.25	49.06	16.4
[10]	$0.187\lambda \times 0.193\lambda$	6.53 : 1	1.7	4070.3	3.96
[11]	$0.154\lambda \times 0.159\lambda$	8.07 : 1	1.4	10173.2	4.6
[12]	$0.28\lambda \times 0.32\lambda$	15.79 : 1	1.9	1966.5	5.6
[13]	$0.30\lambda \times 0.30\lambda$	16.67 : 1	3	1970	10
[14]	$0.34\lambda \times 0.34\lambda$	12.02 : 1	2.59	1422.4	5
[15]	$0.32\lambda \times 0.34\lambda$	11 : 1	3.4	1531.9	11
[16]	$0.18\lambda \times 0.23\lambda$	15.38 : 1	1.3	4261	5.35
[17]	$0.075\lambda \times 0.12\lambda$	24.8 : 1	0.9	20502	4.25
[18]	$0.25\lambda \times 0.29\lambda$	14.32 : 1	2.76	2398.6	6.88
[19]	$0.18\lambda \times 0.27\lambda$	11.6 : 1	2.5	3462	6.1
<b>Proposed Antenna</b>	<b><math>0.053\lambda \times 0.083\lambda</math></b>	<b>30 : 1</b>	<b>1</b>	<b>42531.6</b>	<b>5.5</b>

The far field radiation pattern of an antenna is a three-dimensional diagrammatical delineation of the radiation properties of the antenna, which shows the potency of the radiated field into space as a function of direction. The radiation pattern response of the fabricated antenna is measured and compared with the simulated one. Fig. 12 shows the measured and simulated radiation patterns (co- and cross-polarization patterns) at frequencies 4 GHz, 10 GHz, 14 GHz, 22 GHz, and 30 GHz in the  $E$  ( $YZ$ )-plane ( $\phi = 0^\circ$ ) and  $H$  ( $XZ$ )-plane ( $\phi = 90^\circ$ ). From the figure one can notice that the cross polarization performances are  $-30$ ,  $-29$ ,  $-14$ ,  $-10$ , and  $-9$  dB in the  $H$ -plane and  $-60$ ,  $-50$ ,  $-45$ ,  $-32$ , and  $-26$  dB in the  $E$ -plane at the frequencies of 4, 10, 14, 22, and 30 GHz, respectively. It reveals that the antenna has low cross-polarization at frequencies 4, 10, 14, 22, and 30 GHz in both the planes ( $E$ - and  $H$ -planes). Usually, the antenna with low cross-polarization is beneficial for diminishing the multi-path fading effect in multi-path environment. Additionally, the proposed antenna has nearly omnidirectional (uniform radiation in one plane) radiation patterns throughout the passband (1–30 GHz) in  $H$ -plane. On the other hand, a few radiation nulls are noticed at 22 and 30 GHz in both the planes ( $E$ - and  $H$ -planes); however, these radiation nulls are very shallow and have a negligible effect on the antenna performance.

## 6. TIME DOMAIN INVESTIGATION

Time domain behavior is an essential parameter to examine the distortion in pulses caused by an antenna in the Fraunhofer region. This analysis is carried out using Anritsu S820E VNA by placing two analogous antennas (one for radiating and the other for receiving) at a distance of 30 cm in both side-by-side and face-to-face configurations. A 5th-order Gaussian signal (input signal) as a function of time is chosen to stimulate the proposed SWB antenna as displayed in Fig. 13(a), whereas Fig. 13(b)

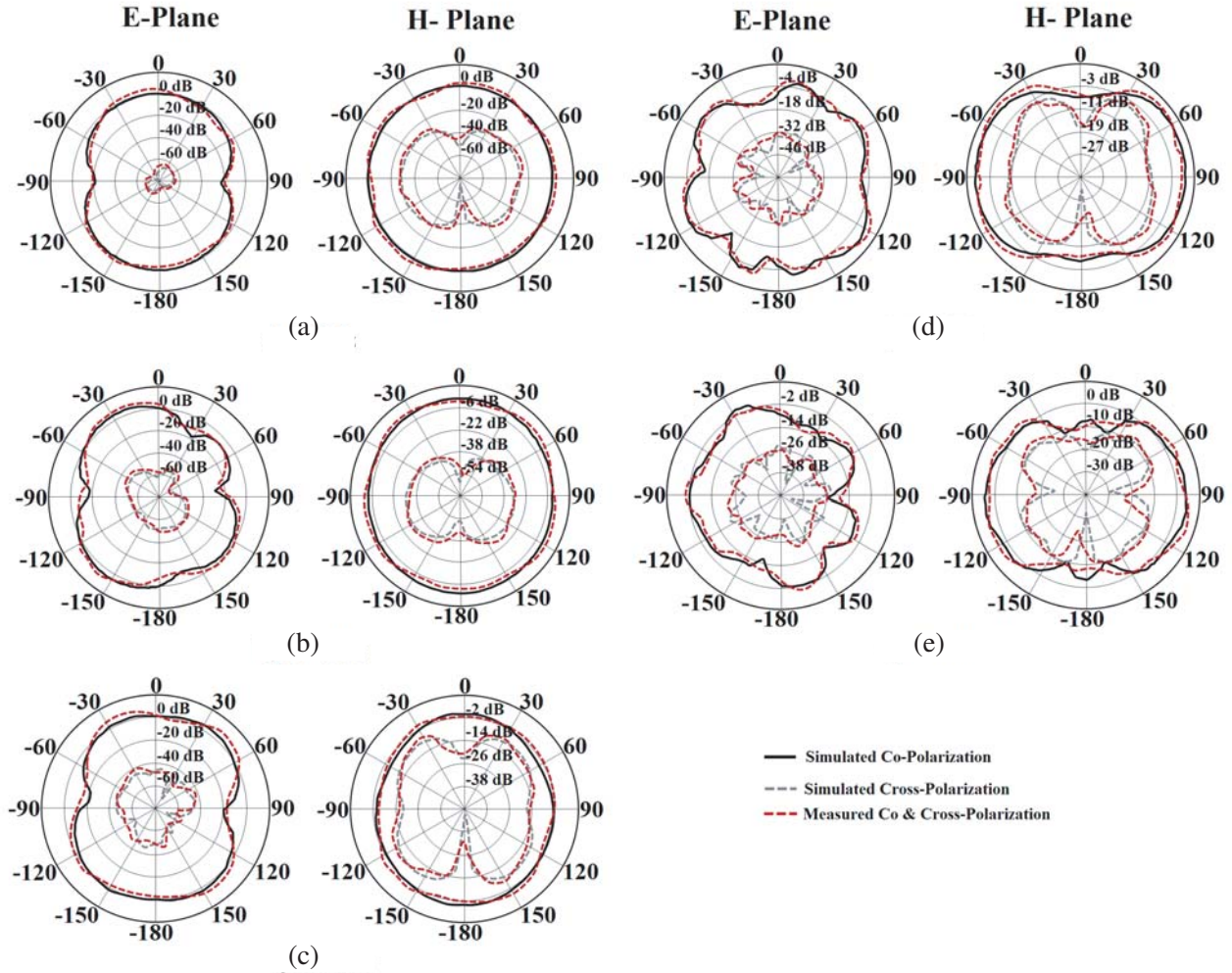


**Figure 12.** Simulated and measured radiation patterns of the proposed SWB antenna for  $E$  ( $YZ$ )-plane and  $H$  ( $XZ$ )-plane at (a) 4 GHz, (b) 10 GHz, (c) 14 GHz, (d) 22 GHz, (e) 30 GHz.

shows the output pulses (convolution of impulse and radiated signals) for the face-to-face and side-by-side arrangements. From Fig. 13(b), it can be seen that the distortion in the received pulse is somewhat more in case of side-by-side arrangement than the face-to-face arrangement. This is owing to the coverage of the entire radiating patch, when the transmitting and receiving antennas are positioned in face-to-face orientation, and hence distortion is less. To inspect the transmitted and received signals strength in the far field region, the group delay functionality is investigated.

Group delay plays a vital role in an SWB communication system, to have minimum differential time delay over the desired band. Group delay is used not only to compute the phase characteristics of filters/amplifiers but also to characterize the phase transfer function of UWB/SWB antenna. The average group delay is described as the ratio of phase derivative to its angular frequency [24, 25]

$$\tau = -dZ(\omega)/d\omega = -\frac{1}{2\pi} \frac{dZ(f)}{d(f)} \tag{8}$$

here,  $Z(\omega)$  is the phase response, and  $\omega$  is the angular frequency. The relation between measured group delay and frequency response over the entire bandwidth is demonstrated in Fig. 14. As observed from the figure, the group delay variations for side-by-side and face-to-face configurations are less than 0.8 ns which validates that the proposed antenna has a linear phase variation in the far-field zone.

In order to examine the resemblance between the excited pulse and received pulse, the system fidelity factor (SFF) is evaluated. It assists the measurement of the cross-correlation during the signal

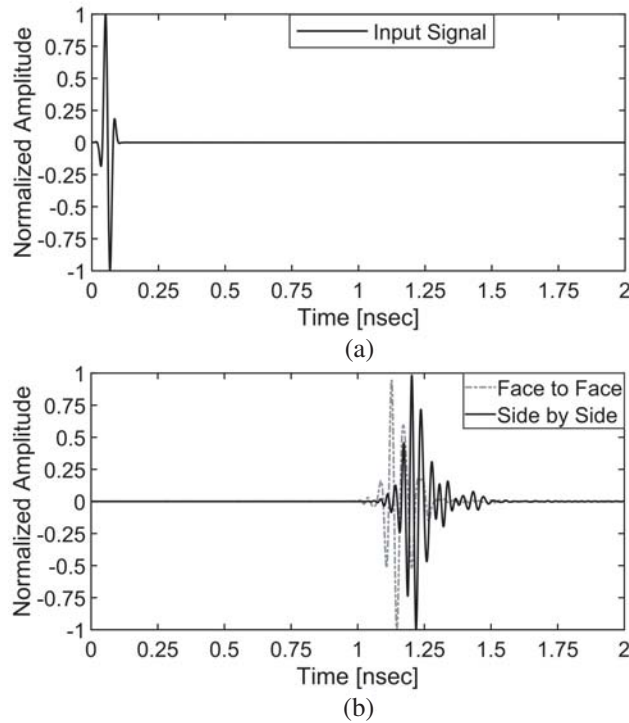


**Figure 13.** Time domain signal response. (a) 5th-order derivative Gaussian pulse. (b) Measured received pulses for both antenna arrangement.

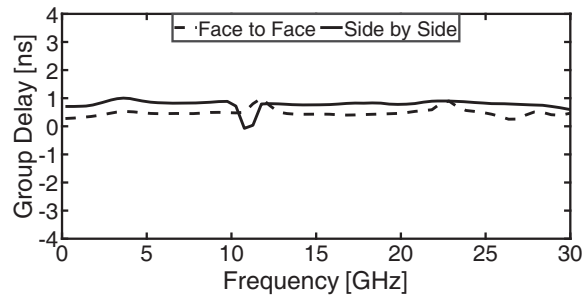


**Figure 14.** Group delay vs frequency response for both antenna configurations.

transmission and reception by adopting the following expressions defined in [26]

$$\hat{E}_p(t) = \frac{E_p(t)}{\left[ \int_{-\infty}^{\infty} |E_p(t)|^2 dt \right]^{1/2}} \quad (9)$$

$$\hat{R}_p(t) = \frac{R_p(t)}{\left[ \int_{-\infty}^{\infty} |R_p(t)|^2 dt \right]^{1/2}} \quad (10)$$

$$FF = \max \int_{-\infty}^{\infty} \hat{E}_p(t) \hat{R}_p(t + \tau) dt \quad (11)$$

where  $\tau$ ,  $\hat{E}_p(t)$ , and  $\hat{R}_p(t)$  denote the signal group delay, excited and received pulses, respectively. The numerical values of SFFs are 0.85 and 0.81 for face-to-face and side-by-side orientations, respectively. This shows that the distortion level is within satisfactory limit (greater than 0.5). If the distortion level falls below 0.5, then it will become difficult to recognize the desired pulse.

## 7. CONCLUSION

In this article, a compact high gain monopole patch antenna is designed, simulated, and analyzed for future handheld gadgets. The presented antenna is miniaturized in size (electrical dimension of  $0.053\lambda \times 0.083\lambda$ ) and has an extremely wide impedance bandwidth of 1–30 GHz with a percentage bandwidth of 187.1%. Furthermore, the proposed antenna has a higher BDR of 42531.6 with a gain variation between 0.1 and 5.5 dBi over the operation band. The equivalent circuit method is used to analyze the proposed antenna which is further verified by the simulated and experimental results. Fairly good correlation values are seen in face-to-face (0.85) and side-by-side (0.81) arrangements. A judiciously good consistency is noticed among analytical, simulated, and experimental outcomes. The proposed SWB antenna is an efficient antenna achieving applications for NB-IoT, GPS, Wi-BRO, ISM band, IRNSS, WiMAX, X-band, Ku-band, and K-band.

## ACKNOWLEDGMENT

The author is deeply thankful to Technical Education Quality Improvement Programme (TEQIP-III) for providing financial assistantship during the research work.

## REFERENCES

1. Anguera, J., A. Andújar, M. C. Huynh, et al., “Advances in antenna technology for wireless handheld devices,” *International Journal on Antennas and Propagation*, Vol. 2013, 2013.
2. Wong, K. L., *Planar Antennas for Wireless Communications*, Wiley Inter-Science, 2003.
3. Rumsey, V., *Frequency Independent Antennas*, Academic Press, New York, 1966.
4. Chen, D. and C. Q. Cheng, “A novel compact Ultra-Wideband (UWB) wide slot antenna with via holes,” *Progress In Electromagnetics Research*, Vol. 94, 343–349, 2009.
5. Haq, M. A. U., S. Koziel, and Q. S. Cheng, “Miniaturisation of wideband antennas by means of feed line topology alterations,” *IET Microwaves, Antennas & Propagation*, Vol. 12, No. 13, 2128–2134, 2018.
6. Dong, Y., W. Hong, and L. Liu, “Performance analysis of a printed super-wideband antenna,” *Microwave and Optical Technology Letters*, Vol. 51, No. 4, 949–956, 2009.
7. Singhal, S. and A. K. Singh, “Elliptical monopole based super wideband fractal antenna,” *Microwave and Optical Technology Letters*, Vol. 62, No. 3, 1324–1328, 2020.
8. Trinh-van, S., G. Kwon, and K. C. Hwang, “Planar super-wideband loop antenna with asymmetric coplanar strip feed,” *Electronics Letters*, Vol. 52, No. 2, 96–98, 2015.
9. Omar, S. A., A. Iqbal, O. A. Saraereh, et al., “An array of M-SHAPED vivaldi antennas for UWB applications,” *Progress In Electromagnetics Research Letters*, Vol. 68, 67–72, 2017.
10. Iqbal, A., O. A. Saraereh, and S. K. Jaiswal, “Maple leaf shaped UWB monopole antenna with dual band notch functionality,” *Progress In Electromagnetics Research C*, Vol. 71, 169–175, 2017.
11. Iqbal, A., A. Smida, N. K. Mallat, et al., “A compact UWB antenna with independently controllable notch bands,” *Sensors*, Vol. 19, No. 6, 1411, 2019.
12. Palaniswami, S. K., M. Kanagasabai, and S. A. Kumar, “Super wideband printed monopole antenna for ultra wideband applications,” *International Journal of Microwave and Wireless Technologies*, Vol. 9, No. 1, 133–141, 2017.
13. Oskouei, H. D. and A. Mirtaheri, “A monopole super wideband microstrip antenna with band-notch rejection,” *2017 Progress In Electromagnetics Research Symposium — Fall (PIERS — FALL)*, 2019–2024, Singapore, Singapore, Nov. 19–22, 2017.

14. Okan, T., "A compact octagonal-ring monopole antenna for super wideband applications," *Microwave and Optical Technology Letters*, Vol. 62, No. 3, 1237–1244, 2020.
15. Singhal, S. and A. K. Singh, "CPW-fed hexagonal Sierpinski super wideband fractal antenna," *IET Microwaves, Antennas & Propagation*, Vol. 10, No. 15, 1701–1707, 2016.
16. Samsuzzaman, M. and M. T. Islam, "A semicircular shaped super wideband patch antenna with high bandwidth dimension ratio," *Microwave and Optical Technology Letters*, Vol. 57, No. 2, 445–452, 2015.
17. Tahir, F. A. and A. H. Naqvi, "A compact hut-shaped printed antenna for super-wideband applications," *Microwave and Optical Technology Letters*, Vol. 57, No. 11, 2645–2649, 2015.
18. Sharma, M., "Superwideband triple notch monopole antenna for multiple wireless applications," *Wireless Personal Communications*, Vol. 104, No. 1, 459–470, 2019.
19. Rahman, M. N., M. T. Islam, M. Z. Mahmud, et al., "Compact microstrip patch antenna proclaiming super wideband characteristics," *Microwave and Optical Technology Letters*, Vol. 59, No. 10, 2563–2570, 2017.
20. Aziz, S. Z. and M. F. Jamlos, "Compact super wideband patch antenna design using diversities of reactive loaded technique," *Microwave and Optical Technology Letters*, Vol. 58, No. 12, 2811–2814, 2016.
21. Manohar, M., R. S. Kshetrimayum, and A. K. Gogoi, "Printed monopole antenna with tapered feed line, feed region and patch for super wideband applications," *IET Microwaves, Antennas & Propagation*, Vol. 8, No. 1, 39–45, 2014.
22. Risco, S., J. Anguera, A. Andújar, et al., "Coupled monopole antenna design for multiband handset devices," *Microwave and Optical Technology Letters*, Vol. 52, No. 2, 359–364, 2010.
23. Chu, Q. X. and Y. Y. Yang, "A compact ultrawideband antenna with 3.4/5.5 GHz dual band-notched characteristics," *IEEE Transactions on Antennas and Propagation*, Vol. 56, No. 12, 3637–3644, 2008.
24. Zhu, X., Y. Li, S. Yong, et al., "A novel definition and measurement method of group delay and its application," *IEEE Transactions on Instrumentation and Measurement*, Vol. 58, No. 1, 229–233, 2008.
25. Mussina, R., D. R. Selviah, F. A. Fernandez, et al., "A rapid accurate technique to calculate the group delay, dispersion and dispersion slope of arbitrary radial refractive index profile weakly-guiding optical fibers," *Progress In Electromagnetics Research*, Vol. 145, 93–113, 2014.
26. Quintero, G., J. F. Zurcher, and A. K. Skrivervik, "System fidelity factor: A new method for comparing UWB antennas," *IEEE Transactions on Antennas and Propagation*, Vol. 59, No. 7, 2502–2212, 2011.